UNIVERSITY of CALIFORNIA
SANTA CRUZ

MICROWAVE ABSORPTION IN NANOSTRUCTURES

A thesis submitted in partial satisfaction of the
requirements for the degree of

BACHELOR OF SCIENCE

in

APPLIED PHYSICS

by

Maxim V. Akhterov

10 June 2010

The thesis of Maxim V. Akhterov is approved by:

Professor Yat Li Advisor	Professor David P. Belanger Senior Theses Coordinator

Professor David P. Belanger
Chair, Department of Physics

Abstract

Microwave Absorption in Nanostructures

by

Maxim V. Akhterov

Absorption of electro-magnetic radiation in a microwave region (300 MHz to 300 GHz) is of high importance in the number of fields in today's civilian and military technology. The rapid development of various wireless electronic devices requires an extensive knowledge of electro-magnetic interference and materials that provide cheap and effective shielding from the unwanted radiation. In aerospace engineering, the development of a lightweight microwave absorber in a broad range of frequencies is an essential part of the *stealth* technology where it is used to minimize the reflection of a radar beam from the aircraft surface. Nanomaterials are promising candidates for electro-magnetic absorbers because of their unique mechanical and electrical properties. Composites based on the nanoscale elements can be lightweight, inexpensive, easy to manufacture and deposit. In this thesis, we discus the theory of electromagnetic absorption and investigate a bi-layered composite absorber with multi-walled carbon nanotubes and iron oxide nanoparticles.

Contents

List of Figures

To my newborn nephew Michael, my brother Alex and his wife Vera.

To my parents who are inspiring me to achieve my goals.

To my girlfriend Anna who is making my life brighter.

Acknowledgements

This research has been an exciting scientific journey, but it would not be possible without the help and assistantship of the following people:

• **Dr. Yat Li** (Chemistry Department): My thesis advisor who welcomed my research endevours and whose invaluable advice helped me throughout the project.

• **Graduate student Mark McDonald** from the group of Dr. Kenneth Pedrotti (Electrical Engineering Department): Our main collaborator and the guru of microwave measurements. Mark's knowledge and experience were essential for making the measurements and developing the software.

• **Graduate student Gongming Wang** from the group of Dr. Yat Li (Chemistry Department): Gongwing helped me numerous times in the chemistry lab and also provided the TEM image of carbon nanotubes (Fig. 3.1b).

• **Graduate student Jason Cooper** from the group of Dr. Jin Zhang (Chemistry Department): Jason helped me to get a great TEM image of iron oxide nanoparticles (Fig. 3.2).

• **Postdoctoral fellow Xunyu Yang** from the group of Dr. Yat Li (Chemistry Department): Xunuy was very helpful in answering my questions about the chemical procedures.

• **Undergraduate student Ethan Amezcua** from the group of Dr. Yat Li (Chemistry Department): Discussions with Ethan were always insightful. His ability to ask basic, but fundamental questions, made me rethink the basic assumptions and further my understanding.

1 Introduction

Today's world heavily relies on the technologies based on electromagnetic radiation - one of the most fundamental phenomena in nature. The extensive study of electromagnetism pioneered by James Clerk Maxwell in the 19th century brought us radio, television, wireless communication, global navigation, radars, and other devices that sustain the needs of our rapidly evolving society. However, as our technological system grows in complexity the unwanted interactions start to happen between its constituents. The phenomenon known as Electromagnetic Interference (EMI) is a disturbance that affects an electrical circuit of a device due to a electromagnetic radiation from another electrical circuit. With the millions of personal electronics in use today it becomes essential to *shield* circuits from unwanted interference in a broad range of electromagnetic frequencies. Furthermore, the ongoing downscaling trend in electronics requires the shielding material to be thin, lightweight, easy to manufacture, and cheap.

Electromagnetic absorption is also of high importance in aerospace engineering where the development of a lightweight absorbing material in a broad range of frequencies is an essential part of the *stealth* technology. An absorber soaks up the incident electromagnetic energy, thereby reducing the net energy available for reflection back to radar. In other words, the more absorptive the material is the more invisible for a radar an aircraft can be. Though the current state of the stealth technology is highly classified, to the best of our knowledge today's Radar Absorbent Materials (RAM) still suffer a trade-off between the broadband effectiveness and the absorber weight that can significantly reduce aircraft's payload. In this thesis, we first establish a theoretical foundation of electro-magnetic absorption in matter. Then we explain how composites based on nano-scale materials enhance the absorption, and finally present our preliminary results on the proposed bi-layered microwave absorber based on multi-walled carbon nanotubes and iron oxide nanoparticles.

2 Theory of Electromagnetic Absorption

Have you ever wondered what makes military aircrafts stealthy? Scientifically, stealth technology is based on the principle of minimizing aircraft's Radar Cross Section (RCS) which is a measure of how detectable an object is with a radar. When a radar beam hits the aircraft surface some energy is reflected and some energy is absorbed. The lower the RCS, the less energy returns to the radar and the more stealthy the aircraft is. There are number of ways to minimize RCS by reducing the size of an object, modifying the shape, or coating the surface with the Radar Absorbent Materials (RAM). This section reviews the theory behind the mechanisms of propagation and loss of electromagnetic energy. Since a radar beam is an electromagnetic wave packet, we start with Maxwell's equations which are fundamental laws governing all electromagnetic behavior.

2.1 Maxwell Equations

Electromagnetic wave consists of a time-varying electric and magnetic field, thereby the study of electromagnetic absorption requires a knowledge of how the fields interact with a material. Let's say the radar's antenna has transmitted a pulse of microwaves of certain frequency and it is propagating through free space. Maxwell equations for electromagnetic waves in the pulse can be written as

$$\begin{aligned} \nabla \cdot \mathbf{E} &= 0 \\ \nabla \cdot \mathbf{B} &= 0 \\ \nabla \times \mathbf{E} &= -\frac{\partial \mathbf{B}}{\partial t} \\ \nabla \times \mathbf{B} &= \mu_0 \epsilon_0 \frac{\partial \mathbf{E}}{\partial t} \end{aligned} \tag{2.1}$$

When an electromagnetic wave from a radar finally hits the aircraft's surface it will produce two waves: reflected and absorbed. We will focus on what happens at an interface in the next section, but now let's rewrite (2.1) for an absorbed wave:

$$\begin{aligned} \nabla \cdot \mathbf{D} &= \rho \\ \nabla \cdot \mathbf{B} &= 0 \\ \nabla \times \mathbf{E} &= -\frac{\partial \mathbf{B}}{\partial t} \\ \nabla \times \mathbf{H} &= \mathbf{J}_f + \frac{\partial \mathbf{D}}{\partial t} \end{aligned} \tag{2.2}$$

where $\mathbf{E}$ is an electric field; $\mathbf{D}$is an electric displacement; $\mathbf{B}$ is a magnetic field; and $\mathbf{J}_f$ is a free current density. The relationships between four vector fields are given by constitutive relations

$$\begin{aligned} \mathbf{D} &= \epsilon_r \epsilon_0 \mathbf{E} \\ \mathbf{H} &= \frac{1}{\mu_r \mu_0} \mathbf{B} \\ \mathbf{J}_f &= \sigma \mathbf{E} \end{aligned} \tag{2.3}$$

Here σ, ϵ, and μ are *conductivity*, *permittivity* and *permeability* of the material respectively. These three properties govern the propagation of electromagnetic waves through the material.

2.2 Boundary conditions

The problem of minimizing radar "imprint" of the aircraft known as Radar Cross Section is inherently a study of what happens when electromagnetic waves transmitted by the radar strike the aircraft surface [1]. This study implies considering boundary conditions, reflection and transmission coefficients. Based on the physical reasoning that a charge can be neither created nor destroyed and that electromagnetic fields are created by charge and current distributions, we conclude that fields in (2.2) must satisfy boundary conditions at the interface between the two media. For two media with permittivities and permeabilities ϵ_1, μ_1 and ϵ_2, μ_2 the boundary conditions for Maxwell

equations take the following form

$$\begin{aligned} \mathbf{D}_{1n} - \mathbf{D}_{2n} &= \rho_s \\ \mathbf{B}_{1n} - \mathbf{B}_{2n} &= 0 \\ \mathbf{E}_{1t} - \mathbf{E}_{2t} &= 0 \\ \mathbf{H}_{1t} - \mathbf{H}_{2t} &= \mathbf{J}_s \times \hat{\mathbf{n}} \end{aligned} \tag{2.4}$$

where ρ_s is the free surface charge, $\mathbf{J}_s$ the free surface current, $\hat{\mathbf{n}}$ is a unit normal outward from the surface (Fig.2.1). Since the aircraft surface has no externally applied chargers or currents, (2.4) may be stated as

$$\begin{aligned} \mathbf{D}_{1n} &= \mathbf{D}_{2n} \\ \mathbf{B}_{1n} &= \mathbf{B}_{2n} \\ \mathbf{E}_{1t} &= \mathbf{E}_{2t} \\ \mathbf{H}_{1t} &= \mathbf{H}_{2t} \end{aligned} \tag{2.5}$$

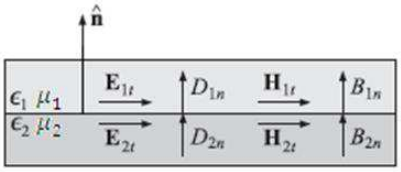

Figure 2.1: Boundary components of electromagnetic field [2].

Equations (2.5) describe the boundary fields between any two media. However, let's be more specific and consider an electro-magnetic wave striking a boundary between a free space and a perfect conductor (aluminum based alloys used in airspace engineering can be approximated to act like one). In general, for any two mediums an incident wave will produce a reflected and transmitted (absorbed) wave. As shown in Fig.2.2. a monochromic plane wave traveling in free space in z direction and polarized in the x direction hits the conductor from the left

$$\left.\begin{aligned} \mathbf{E}_I(z,t) &= \mathbf{E}_{0_I} e^{i(k_1 z - \omega t)} \hat{\mathbf{x}} \\ \mathbf{B}_I(z,t) &= \tfrac{1}{v_1} \mathbf{E}_{0_I} e^{i(k_1 z - \omega t)} \hat{\mathbf{y}} \end{aligned}\right\} \tag{2.6}$$

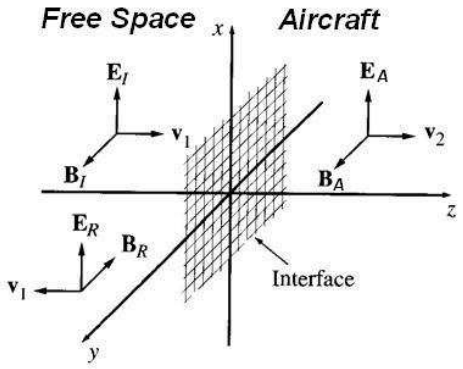

Figure 2.2: Interface between a free space and an aircraft surface. Incident radar wave creates a reflected and absorbed wave [3].

The incident wave creates a reflected wave propagating to the left in free space

$$\left.\begin{aligned}\mathbf{E}_R(z,t) &= \mathbf{E}_{0_R} e^{i(-k_1 z-\omega t)}\hat{\mathbf{x}} \\ \mathbf{B}_R(z,t) &= -\tfrac{1}{v_1}\mathbf{E}_{0_I} e^{i(-k_1 z-\omega t)}\hat{\mathbf{y}}\end{aligned}\right\} \tag{2.7}$$

and an absorbed wave which is attenuated as penetrates into the aircraft body

$$\left.\begin{aligned}\mathbf{E}_A(z,t) &= \mathbf{E}_{0_A} e^{i(k_2 z-\omega t)}\hat{\mathbf{x}} \\ \mathbf{B}_A(z,t) &= \tfrac{1}{v_2}\mathbf{E}_{0_A} e^{i(k_2 z-\omega t)}\hat{\mathbf{y}}\end{aligned}\right\} \tag{2.8}$$

At $z = 0$, the combined wave in the free space must join the wave in the aircraft body, pursuant to boundary conditions (2.5). The first and second equation in (2.5) are satisfied since $\mathbf{D}_n = 0$ and $\mathbf{B}_n = 0$ on both sides. Meanwhile, the third boundary condition in (2.5) gives

$$E_{0_I} + E_{0_R} = E_{0_A} \tag{2.9}$$

The fourth boundary condition yields

$$\frac{1}{\mu_0 v_1}(E_{0_I} - E_{0_R}) = \frac{k_2}{\mu_a \omega} E_{0_A} \tag{2.10}$$

or

$$E_{0_I} - E_{0_R} = \beta E_{0_A} \tag{2.11}$$

where

$$\beta = \frac{\mu_0 v_1}{\mu_a \omega} k_2 \tag{2.12}$$

it follows that

$$E_{0_R} = \left(\frac{1-\beta}{1+\beta} E_{0_I}\right), \quad E_{0_A} = \left(\frac{2}{1+\beta} E_{0_I}\right) \tag{2.13}$$

In a perfect conductor conductivity is infinite, so the wave vector k is also infinite, since

$$k \equiv \omega\sqrt{\frac{\epsilon\mu}{2}}\left[\sqrt{1+\left(\frac{\sigma}{\epsilon\omega}\right)^2}+1\right]^{1/2}$$

Hence, it follows from (2.11) that $\beta = \infty$ and (2.10)

$$E_{0_R} = -E_{0_I}, \quad E_{0_A} = 0 \tag{2.14}$$

Thus the EM wave from a radar is totally reflected, with a 180° phase shift. From (2.14) it also follows that on a surface of a conductor the tangential part of E-field goes to zero, while from (2.10) it becomes apparent that the tangential B-field doubles (Fig. 2.3). In Chapter 3, we will use this phenomenon to design a multi-layered RAM with a magnetic material placed near the conductive surface to enhance the absorption of a magnetic field.

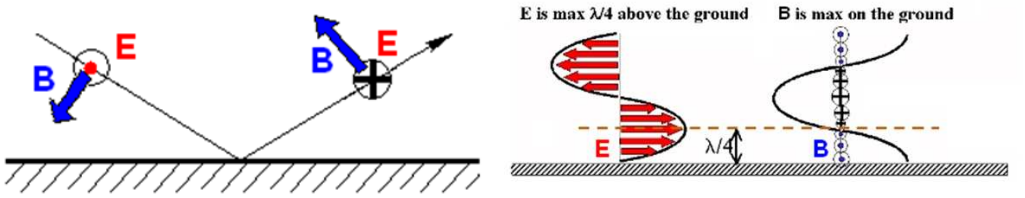

Figure 2.3: E-field is zero at the surface and is maximum at quarter of a wavelength above the conductor, while B-field is maximum at the surface [4].

2.3 Absorption Mechanisms

Radar absorbing materials absorb energy from the electromagnetic fields passing through them. Similar to a resistor that consumes energy of an electric current, RAM dissipates the absorbed EM energy into heat. Since EM wave has an electric and magnetic component, it is common to separate dielectric and magnetic absorption mechanisms. Using Gauss's and Amperes's laws formulated in (2.2) we can derive the energy stored in the electric and magnetic fields of an absorbed EM wave. The energy densities inside the absorber are

$$u_e = \frac{1}{2}\epsilon_A\epsilon_0\left|\mathbf{E}\right|^2 \tag{2.15}$$

$$u_m = \frac{1}{2\mu_A\mu_0}\left|\mathbf{B}\right|^2 \tag{2.16}$$

It follows that relative permittivity ϵ_A and permeability μ_A define RAM's electromagnetic loss. Both numbers are complex and depend on the frequency of an electromagnetic wave

$$\epsilon_A(f) = \epsilon'_A + i\epsilon''_A \tag{2.17}$$
$$\mu_A(f) = \mu'_A + i\mu''_A$$

where the real part (denoted by a prime) is a measure of how much energy from an external electric/-magnetic field is stored in a material; the imaginary part (denoted by a double prime) is called the loss factor and is a measure of how dissipative or lossy a material is to an external electric/magnetic field. Because the absorber's conductivity σ is often the major loss mechanism, it is convenient to express this effect in terms of ϵ''_A

$$\epsilon''_A = \frac{\sigma}{\omega\epsilon_0} \tag{2.18}$$

where $\omega = 2\pi f$ is the radian frequency. In fact, a metal ($\sigma \approx 10^7 Sm^{-1}$) is a highly lossy absorber, however as will be shown in the subsection 2.3.2 and section 2.4, it is also highly reflective. Equivalently, we can rewrite (2.17) in polar notation

$$\epsilon_A(f) = |\epsilon_A|\, e^{i\delta} \tag{2.19}$$
$$\mu_A(f) = |\mu_A|\, e^{i\delta_m}$$

where δ and δ_m are the electric and magnetic loss tangents given by

$$\tan\delta = \frac{\epsilon''_A}{\epsilon'_A} \tag{2.20}$$
$$\tan\delta_m = \frac{\mu''_A}{\mu'_A}$$

We can interpret loss tangent as a ratio of energy lost per cycle to energy stored per cycle. However, the fundamental question is "Why is energy dissipated in an absorber?".

2.3.1 Electric field loss

An absorption of electric field in matter is due to the number of dielectric mechanisms or polarization effects that contribute to the overall permittivity ϵ_A. In a microwave region, the loss is caused primarily by the dielectric relaxation effects associated with permanent and induced molecular dipoles. The electrical field E creates a torque T on the electric dipole, and the dipole rotates to

align with the electric field, thus creating **orientation polarization** (Fig.2.4). At low frequencies electric field changes slowly and the dipole has enough time to align, but at microwave frequencies dipole's alignment starts to lag due to the viscosity of the material. The friction accompanying the alignment of the dipole leads to energy dissipation in a form of heat. Water is an example of a substance that exhibits strong orientation polarization (H_2O is a polar molecule, meaning it has a permanent dipole moment) and that is why food heats in a microwave oven.

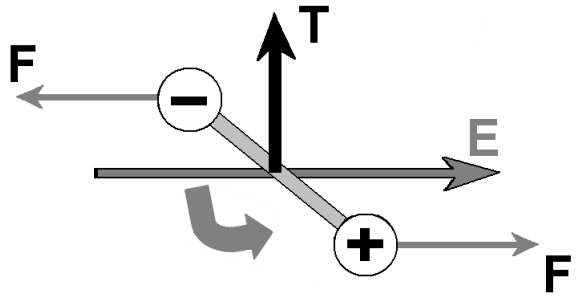

Figure 2.4: Dipole alignment with an electric field.

In terms of permittivity, the rotation of dipoles leads to a variation in both ϵ'_A and ϵ''_A at the relaxation frequency f_c, which is related to the time τ (called "relaxation time") required for an aligned dipole in an electric field to return to $1/e$ of its random equilibrium value

$$\tau = \frac{1}{2\pi f_c} \tag{2.21}$$

At frequencies below f_c when dipoles can keep up with the a pace of field variations, the loss ϵ''_A is directly proportional to the frequency. As the frequency increases, ϵ''_A continues to increase, but the storage of electric energy ϵ'_A begins to drop due to the lack of alignment between the dipole and an electric field. At frequencies above f_c the field is oscillating too fast to affect polarization, so both parts of a complex permittivity decrease. The described dependency of permittivity as function of frequency for ideal dipoles is known as Debye relaxation model (Fig.2.5)

One other type of polarization we need to consider in our study of microwave absorption in nanostructures is **interfacial** or **space charge polarization**. When an absorber is made of more than one material (heterogeneous system), the free charge carriers cannot fully migrate through the material in the presence of an electric field. The carriers can be trapped within the absorber's interfaces and cause the accumulation of charges, which distorts the electric field and increases the overall material's capacitance, thereby increasing ϵ'_A.

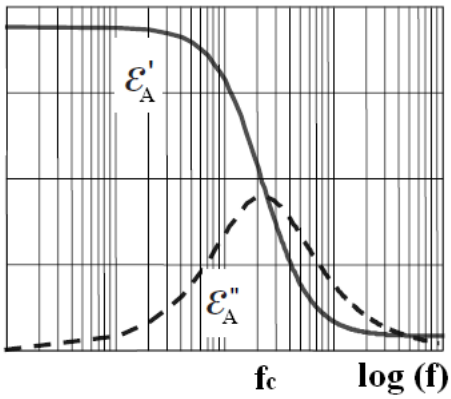

Figure 2.5: Debye relaxation spectra [7].

2.3.2 Magnetic field loss

Ferrites are iron oxide based compounds commonly employed as magnetic absorbers in RAM design. Similar to the absorption of an electric field, different magnetic loss mechanisms dominate at different frequencies. At lower frequencies of magnetic field energy is dissipated as heat caused by the magnetic dipoles re-alignment [6]. This phenomenon known as **hysteresis** reflects the non-linear relationship between the applied magnetic field intensity H and the magnetization of the material M. The two important parameters of this loss mechanism are saturation magnetization (maximum possible magnetization of the material) and coercivity (field required to reduce magnetization to zero) (Fig.2.6).

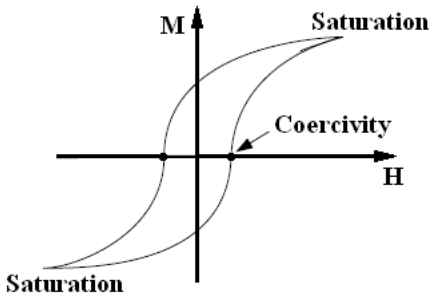

Figure 2.6: Hysteresis loop.

As we have seen in (2.18) and (2.20) material's conductivity increases the electric loss. It also plays an important role in a magnetic loss due to the **eddy currents**. For eddy currents to occur material has to have a large conductivity and thickness larger than the skin depth δ, which is defined as the depth of penetration of the magnetic field at which its value decreases by $1/e$ of its surface value ($\delta = \sqrt{\frac{2}{\sigma\omega\mu}}$). From the third Maxwell's Equation in (2.2) it follows that the

alternating magnetic field generates an electric field that drives the charge carriers via the Lorentz force ($\mathbf{F}_L = q\mathbf{E}$). The resulting eddy current dissipates energy in a form of heat. However, as any other alternating current, it also re-emits an EM wave that can be easily detected - this makes metals highly reflective.

In a microwave region the residual losses due to resonance effects often dominate [5]. The resonance phenomenon has two distinct loss mechanisms: magnetic **domain wall resonance** and **ferromagnetic resonance**. A magnetic domain is a region within a material that has magnetic moments of atoms aligned in one direction that creates a uniform magnetization within a domain. When an external magnetic field is applied the domain's wall is slightly displaced and the lattice strain creates the restoring force. Since the wall has inertia the movement is accompanied by energy dissipation and an equation of motion can be written for a sinusoidal applied field [6]

$$m\ddot{x} + \beta\dot{x} + kx = 2M_s B(t) \tag{2.22}$$

where x is the displacement normal to the wall, m is inertia, β is a damping coefficient, k is a stiffness coefficient, M_s is a saturation magnetization, and $B(t)$ is an alternating magnetic field. Equation (2.22) describes a damped harmonic oscillation and, if damping is small, a resonance effect will occur at a frequency $\omega = \sqrt{\frac{k}{m}}$.

Ferromagnetic resonance (FMR) is complicated phenomenon which is beyond the scope of this thesis and the following description is meant only to familiarize a reader with the main idea (for more information about FMR we recommend [8-10]). In ferromagnetic and ferrimagnetic materials, the spin of an electron combined with its electric charge results in a magnetic dipole moment and creates a magnetic field that contributes to the overall material's magnetization. Since the magnetic moment is associated with an angular momentum, in a static magnetic field[1] the electron experiences a torque and precesses around the field direction with the Larmor angular frequency

$$f_L = \frac{\gamma\mu_0}{2\pi} H = 35.2 \times 10^6 H \quad (GHz) \tag{2.23}$$

where γ is the gyroscopic ratio ($\gamma = \frac{g\mu_b}{h} = 1.76 \times 10^{11} \quad T^{-1}s{-}1$), H is the magnetic field (A/m) [6]. If a microwave field of resonance frequency f_L is applied perpendicular to the direction of the static field H, then the torque will cause the angle of precession to increase, so the energy of the

[1] The field can be external or a local anisotropy field

microwave field will be absorbed. When a microwave field is removed the precessional energy will be dissipated, and the magnetization vector gradually spirals towards the direction of the static field (Fig.2.7).

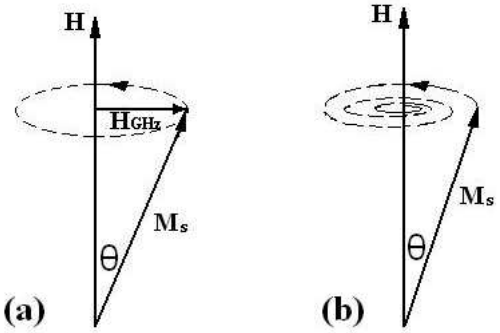

Figure 2.7: Precessional motion of magnetization: (a) precession maintained by an applied microwave field H_{GHz}; (b) M_s spiraling into line with H as the precessional energy is dissipated [6].

In summary, it is important to note that as we have seen magnetic loss mechanisms are intrinsically narrow band. Furthermore, the losses are greater at the lower frequencies, and at the higher frequencies the electric properties of a material account for the electromagnetic absorption. Since relative permittivity and permeability account for the loss mechanisms, we can graphically illustrate their approximate behavior in a microwave region (Fig.2.8).

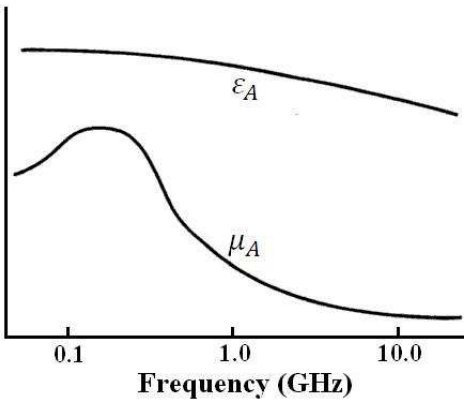

Figure 2.8: Schematic illustration of the frequency behavior of ferrites [1].

2.4 Wave Impedance and Reflectivity

In the previous section we discussed separately electric and magnetic losses, however in practice we do not deal with purely electric of magnetic absorbers, but have a combination of

various loss mechanisms. Therefore, we are interested in cumulative absorption effects, and it is common to describe RAM's performance in terms of its wave impedance and reflectivity.

For any interaction of electromagnetic wave with an aircraft we can define a reflection (R) and absorption (A) coefficients defined by reflected and absorbed electric fields

$$R = \frac{E_{0_R}}{E_{0_I}}, A = \frac{E_{0_A}}{E_{0_I}} \tag{2.24}$$

When the incidence angle is normal to the interface expressions (2.24) can be re-written as

$$R = \frac{Z_A - Z_0}{Z_A + Z_0}, A = \frac{2Z_A}{Z_A + Z_0} \tag{2.25}$$

where

$$Z_A = \sqrt{\frac{j\omega\mu_A}{\sigma_A + j\omega\epsilon_A}}, \quad Z_0 = \sqrt{\frac{\mu_0}{\epsilon_0}} \tag{2.26}$$

are called *wave impedances* of aircraft body and free space respectively. Since for free space $\epsilon_0 = 8.85 \times 10^{-12}$ F m^{-1} and $\mu_0 = 1.26 \times 10^{-6}$ H m^{-1}, then $Z_0 = 377\Omega$. The surface of an aircraft without a RAM is highly conductive ($\sigma_A \to \infty$), so from (2.26) it follows that the wave impedance in the body is very low, $Z_A \Rightarrow 0$. Hence, $R \to -1$ and $A \to 0$, meaning that the wave is entirely reflected and suffers a phase change of 180°.[2] The goal of the stealth technology is to minimize R and maximize A, so an ideal EM absorber would have $Z_A = Z_0 = 377\Omega$, resulting in $R \to 0$ and $A \to 1$, meaning that no reflection occurs and a wave is entirely absorbed. In discussing reflection coefficients of different materials it is common to operate with the power notation of a reflected signal

$$|R|\,(dB) = 20\log_{10}|R| \tag{2.27}$$

which is referred as *reflectivity*.

Rule of thumb: *An absorber with -12dB reflectivity allows the target to get twice as close to the radar before being detected, compared to an object with 0dB reflectivity [4].*

Equations (2.25) and (2.26) suggest that wave propagation in any material depends on its conductivity, permittivity and permeability. However, since RAM with dielectric materials has lower reflectivity, it is common to write absorber's wave impedance in (2.26) as

$$Z_A = \sqrt{\frac{\mu_A}{\epsilon_A}} \tag{2.28}$$

[2]The same results for reflection and absorption coefficients also follow from (2.14) and (2.24)

In our study, we used the metal-backed absorber model to calculate the normalized wave impedance of the RAM:

$$Z_{RAM} = \sqrt{\frac{\mu_r}{\epsilon_r}} \tanh\left(j\frac{2\pi f d}{c}\sqrt{\mu_r \epsilon_r}\right) \tag{2.29}$$

then reflectivity

$$R = \frac{Z_{RAM} - 1}{Z_{RAM} + 1} \tag{2.30}$$

Since relative permittivity μ_A and permeability ϵ_A are frequency dependent (Equations (2.17)), the objective of RAM design is to produce a material for which $|R|$ remains as small as possible over a wide frequency range.

3 Nanostructures

Design of a radar absorbent material is an engineering challenge, since there are number of performance requirements as well as limitations. An ideal RAM should have a low reflectivity (less than -15db) in a wide frequency range (0.5 - 18 GHz), and it should be lightweight, mechanically stable, cheap and easy to deposit. To achieve a broadband performance a multi-layered absorbing structure containing a combination of various absorbing materials can be designed [1]. Each layer then would have a unique set of electromagnetic properties causing an absorption resonance at a certain frequency. However, the downside of existing "hybrid" RAMs is their thickness and weight that can significantly reduce the aircraft's payload. Nanoscale structures with there high surface-to-volume ratio and adjustable electromagnetic properties can be potentially used to resolve the trade-off [11]. In this thesis, we present the first results of our ongoing research of microwave properties of a bi-layered structure containing multi-walled carbon nanotubes and iron (II,III) oxide[1] nanoparticles. Potentially such a configuration can serve as a proof-of-concept for a high performance hybrid EM absorber based on nanomaterials that employ both dielectric and magnetic loss mechanisms.

3.1 Carbon Nanotubes

Carbon nanotubes (CNT), discovered in 1991 by S. Iijima have been attracting scientific interest for almost two decades due to their unique electrical, mechanical, optical, and thermal properties [12,13]. Previous studies on microwave absorption properties of CNTs revealed great reduction in reflectivity in 8-12GHz region (less than -20dB) even for low concentrations (less than %5 wt.) [14-16]. In our research we used CVD[2] grown multi-walled carbon nanotubes (MWCNTs)

[1] Fe_3O_4 is also known as "magnetite" - the most magnetic of all naturally occurring minerals.

[2] Chemical Vapor Deposition (CVD) is the most common method for the commercial production of carbon nanotubes. It involves heating a metal catalyst material to 700-1000°C and introducing a blend of two gases: a carrier gas (ammonia, nitrogen, or hydrogen) and a carbon-containing gas (acetylene, ethylene, ethanol, or methane).

to make a dielectric absorber of the bi-layered RAM. MWCNT consists of multiple layers of graphite rolled in a concentric fashion (Fig.3.1a). MWCNT powder of %95 purity purchased from AlfaAesar contains nanotubes of the following dimensions: 3-20 nm outer diamer, 1-3 nm inner diameter, 0.1-10 micron long (Fig.3.1b). From the section 2.3 we know that absorber's conductivity is proportional

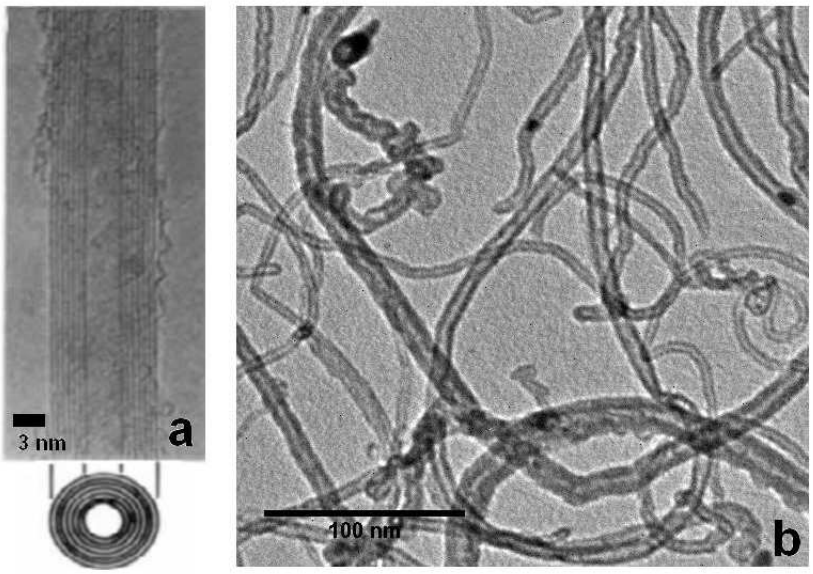

Figure 3.1: a: TEM image of a single MWNT [12] b: TEM image of MWCNTs used [G.Wang].

to the loss factor (Equation 218).However, if the absorber's thickness is larger than the skin depth then the alternating magnetic filed create undesirable eddy currents that increase the reflectivity. MWCNTs can resolve this problem, since they act like tiny conducting wires while being much smaller than the skin depth. Furthermore, because of their high surface-to-volume ratio a collection of surface charges offers a higher interfacial polarization than of a bulk material, thus providing an additional energy loss.

3.2 Fe_3O_4 Nanoparticles

Fe_3O_4 is a ferrimagnetic[3] material that has been widely for preparation of magnetic fluids and biomedical applications [17,18]. Recently, magnetic properties of Fe_3O_4 nanoparticles have been shown to be size dependent [19] and to experience a resonance in a microwave region. The high electric resistivity ($4 * 10^{-3} \Omega m$), large saturation magnetization (0.6T bulk)[20],and higher Snoek's

[3]Ferrimagnetism is similar to ferromagnetism, but the magnetic moments are unequal and point in opposite directions resulting in a net magnetization

limit [21][4] In our research we used Fe_3O_4 synthesized in our lab to make a magnetic absorber of the bi-layered RAM.

The Fe_3O_4 nanoparticles were synthesized by hydrolysis of an aqueous solution containing iron salts and a base at room temperature using method described in [19]. First solution contained 0.017 mol dm^{-3} of ferrous sulfate ($FeSO_4 \cdot 7\,H_2O$) and 0.033 mol dm^{-3} of ferric sulfate ($Fe_2(SO_4)_3 \cdot 7\,H_2O$). Second solution contained 0.25 mol dm^{-3} of 1,6-hexanediamine ($H_2N(CH_2)_6NH_2$). Then, an iron salt solution was mixed with an aqueous solution of 1,6-hexanediamine and black precipitate was immediately produced. After vigorous stirring for 24 hours, the precipitate was washed with water and centrifuged several times. After drying in the oven at 60° the Fe_3O_4 nanoparticles were finally collected. The TEM analysis revealed that the average diameter of the nanoparticles was about 20-25nm (Fig.3.2 a,b).

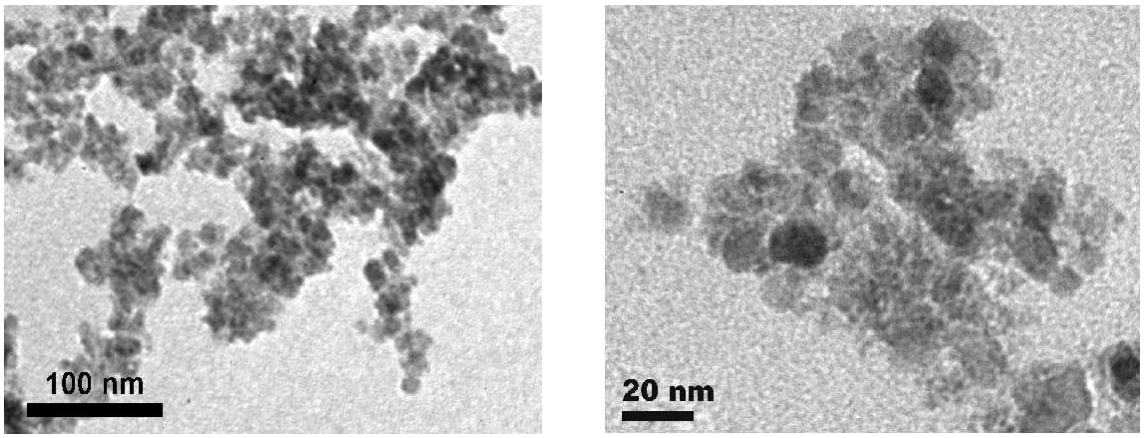

(a) (b)

Figure 3.2: TEM images of synthesized Fe_3O_4 nanoparticles.

3.3 Sample Preparation

First, the powder containing nanomaterial was dispersed in a melted paraffin wax using ultrasonic bath. Then, two samples of a toroidal shape (outer diameter: 8.0 mm, inner diameter 3 mm; thickness: 5.0 mm) were prepared using a Teflon mold. Six sample disks were prepared for microwave measurements with pure paraffin wax, MWNT (%5wt.), and Fe_3O_4 (%5wt.).

[4]Snoek's limit says that the product of the resonance frequency and the initial permeability is approximately constant.

4 Transmission Line Measurements

4.1 Coaxial waveguide

In our study, permittivity and permeability were measured using the coaxial transmission line method. A commercial N-type barrel adapter was modified to serve as a sample holder by removing the inner dielectric. For each measurements two samples containing the material under test (MUT) were placed in a sample holder [1] (Fig.4.1).

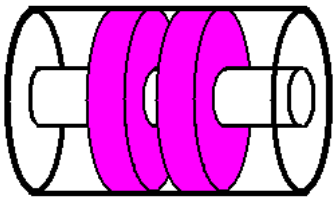

Figure 4.1: Two MUT samples are placed in a coaxial sample holder.

The vector network analyzer (VNA), Agilent 8510C, was used to measure the two-port response in the transmission line. In a sample holder, since the outer conductor is grounded, the alternating current in the inner conductor created by the VNA produces a transverse electromagnetic wave of a certain frequency(Fig.4.2). As the wave travels through the sample holder part of the wave gets reflected, because of the impedance mismatch, and the other gets transmitted. The relationship between the incident, reflected and the transmitted power can be expressed in terms of scattering (S) parameters.

[1] The samples must fit tightly within the sample holder to minimize the measurement error caused by the air gaps.

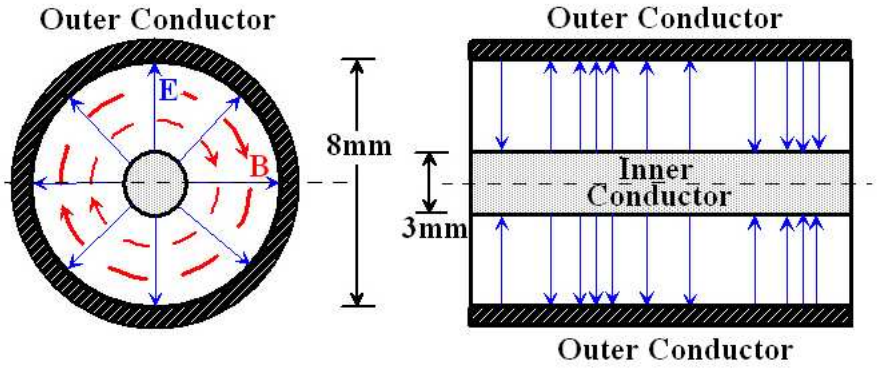

Figure 4.2: Electric field lines are radial and magnetic field lines are circumferential in the coaxial sample holder. Energy of the TEM wave is constrained between the inner and outer conductors [22].

4.2 Scattering parameters

The scattering matrix is the mathematical concept that fully describes the propagation of an electromagnetic wave through a multi-port network. For a signal incident on one port some fraction of the signal bounces back out of that port, some of it scatters and exits other ports, and some of it disappears as heat [23]. The S-matrix for a two-port device has 4 coefficients known as s-parameters that represent all possibles input-output signal paths. The fist number in the subscript of the s-parameter refers to the responding port, while the second represents the incident port (Fig. 4.3).

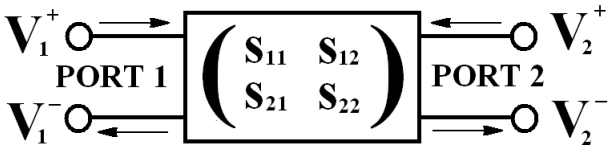

Figure 4.3: Generalized two-port network.

Assuming that each port has a characteristic impedance Z_0, we can define the four s-parameters of a two-port device as

$$\begin{aligned} S_{11} &= \frac{V_1^-}{V_1^+} \\ S_{12} &= \frac{V_1^-}{V_2^+} \\ S_{21} &= \frac{V_2^-}{V_1^+} \\ S_{22} &= \frac{V_2^-}{V_2^+} \end{aligned} \tag{4.1}$$

Each s-parameter in (4.1) is a unitless complex number that represents magnitude and angle, because

both the magnitude and phase of the input signal are changed by the VNA. Once the s-parameters of the coaxial sample holder with the samples are found, the permittivity and permeability of the MUT can be calculated.

4.3 Nicolson-Ross-Wier (NRW) Model

The NRW method is a common technique for calculating material's electromagnetic properties from the s-parameters [24,25]. It requires at least two measured parameters (S_{11} and S_{21}) and works well for lossy materials and short[2] samples. The method is deduced from the following two equations for S_{11} and S_{21}

$$\begin{aligned} S_{11} &= \frac{\left(1-T^2\right)\Gamma}{1-\Gamma^2T^2} \\ S_{21} &= \frac{\left(1-\Gamma^2\right)T}{1-\Gamma^2T^2} \end{aligned} \tag{4.2}$$

where Γ is a reflection coefficient

$$\Gamma = \frac{\sqrt{\frac{\mu_r}{\epsilon_r}}-1}{\sqrt{\frac{\mu_r}{\epsilon_r}}+1} \tag{4.3}$$

and T is a transmission coefficient

$$T = \exp\left[-i\frac{\omega}{c}\sqrt{\mu_r\epsilon_r}d\right] \tag{4.4}$$

here $\omega = 2\pi f$ is the angular frequency, c is the speed of light, and d is the thickness of the sample. Therefore, we can find both of the coefficients from the s-parameters

$$\begin{aligned} V_1 &= S_{21} + S_{11} \\ V_2 &= S_{21} - S_{11} \end{aligned} \tag{4.5}$$

and if

$$X = \frac{1-V_1V_2}{V_1-V_2} \tag{4.6}$$

[2]The sample optimum thickness is $\frac{\lambda_g}{4}$, where $\frac{1}{\lambda_g}$ =Re$\left(\frac{1}{\sqrt{\frac{\epsilon_r\mu_r}{\lambda_0^2}-\frac{1}{\lambda_c^2}}}\right)$, λ_c- cutoff frequency ($\lambda_c = \infty$ for the coaxial transmission line) and λ_0- frequency in GHz

then

$$\Gamma = X \pm \sqrt{X^2 - 1} \tag{4.7}$$

$$T = \frac{V_1 - \Gamma}{1 - V_1\Gamma} \tag{4.8}$$

The appropriate sign should be chosen in (4.7) so that $|\Gamma| \leq 1$.

Now, from (4.3) we define

$$\frac{\mu_r}{\epsilon_r} = \left(\frac{1+\Gamma}{1-\Gamma}\right)^2 = c_1 \tag{4.9}$$

and from (4.4) we define

$$\mu_r\epsilon_r = -\left\{\frac{c}{\omega d}\ln\left(\frac{1}{T}\right)\right\}^2 = c_2 \tag{4.10}$$

Then,

$$\mu_r = \sqrt{c_1 c_2} \tag{4.11}$$

$$\epsilon_r = \sqrt{\frac{c_2}{c_1}} \tag{4.12}$$

The described algorithm was implemented in MatLab. A graphical user interface (GUI) was developed for an easy data input and read-out. The code is presented in Appendix B.

4.4 Measurement Procedure

1. Two MUT samples were positioned in the sample holder as close to each other as possible. There were four pairs of samples: paraffin - paraffin, MWCNTs (%5wt.) - MWCNTs (%5wt.), Fe_3O_4 (%5wt.) - Fe_3O_4 (%5wt.), MWCNTs (%5wt.) - Fe_3O_4 (%5wt.)
2. Each of port of the VNA was calibrated using an open circuit, a short circuit, and a matched 50-ohm load.
3. The sample holder was connected to the transmission line and s-parameters were measured from 1 to 18GHz with 800 test points. The step was repeated for each pair of samples.
4. Data were transfered to a PC and reformatted using a MatLab function format_data.m (see the code in Appendix A).
5. Material Analysis software was run to perform the de-embedding[3] and calculations of permittivity and permeability.

[3]De-embedding with OPEN is used to shift the reference planes closer to the sample surface and minimize, thus minimizing the errors due to the sample holder itself.

5 Data Analysis

5.1 Paraffin wax

Paraffin wax was used as a binding matrix to measure microwave properties of CNT and Fe_3O_4 nanoparticles. However, since paraffin is a dielectric material (dielectric constant = 2.2) itself, it will have some absorption in a microwave region. The Figure 5.1 shows the real and complex parts of the permittivity and the figure 5.2 presents the reflectivity of paraffin. The two highest peaks of reflectivity (-16dB and -18dB) at 13.8GHz and 14.7GHz are due to the polarization of paraffin molecules which leads to energy dissipation and increase of the complex permittivity.

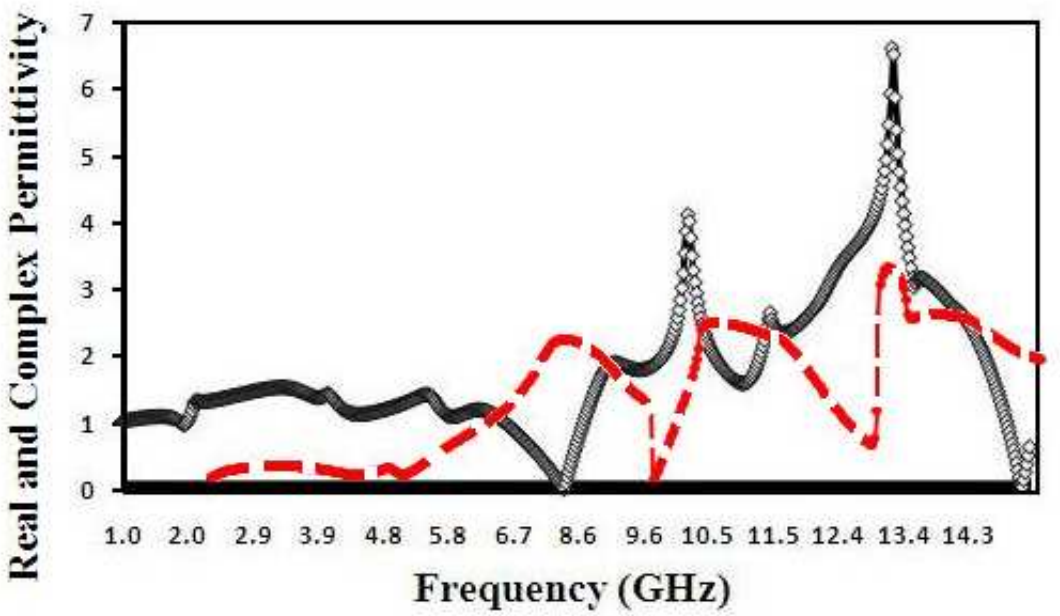

Figure 5.1: Real (solid) and complex (dashed) parts of paraffin's permittivity.

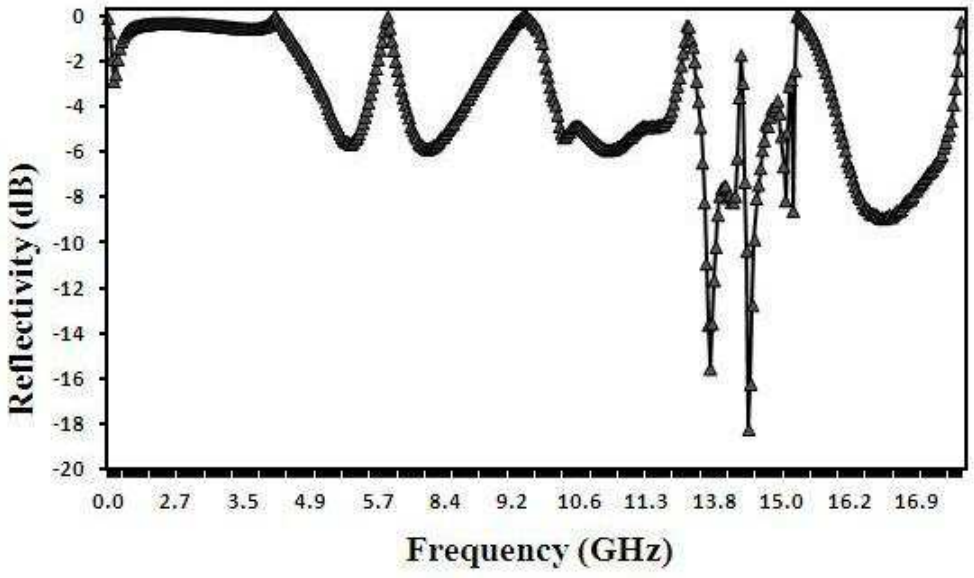

Figure 5.2: Reflectivity of a pure paraffin wax.

5.2 MWCNT (%5wt.)

In our study, we found that purchased MWCNT powder exhibited magnetic properties. Though carbon nanotubes themselves are non-magnetic, the iron catalyst used for the CVD synthesis is ferromagnetic (on a TEM image in the Fig.3.1b iron catalyst is shown as black particles inside the nanotubes). Therefore, we used the NRW method to calculate both electric loss tangent and magnetic loss tangent (Equation 2.20) shown on Figures 5.3 and 5.4. The Figure 5.5 shows the reflectivity of %5wt. MWCNT sample. Using these three graphs we can identify absorption peaks due to the dielectric or magnetic properties of a material. The highest reflectivity peak of -34dB at 14.7GHz is due to the dielectric loss that we believe might be caused by the interfacial polarization, as well as high conductivity of MWCNTs. The second highest absorption peak of -32dB at 16.3GHz is associated with the peak on a magnetic loss tangent. Since this peak is very sharp we suggest that it is due to the ferromagnetic resonance of the iron catalyst that occurs at this particlular frequency. Finally, the third highest reflectivity peak of -23dB at 10.6GHz can be a combination of a dielectric and magnetic loss, since both tangents have peaks around 10GHz.

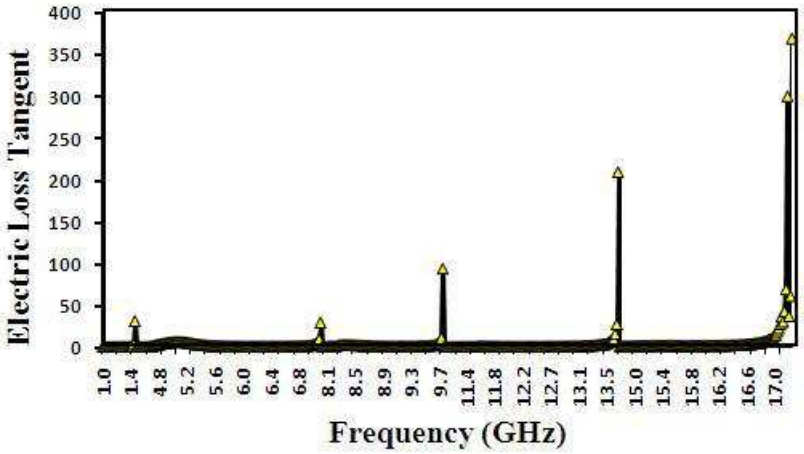

Figure 5.3: MWCNT (%5wt.): Electric Loss Tangent.

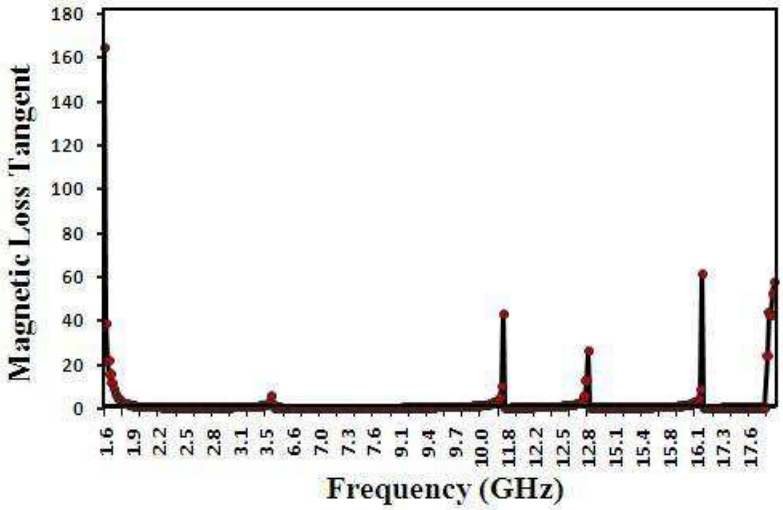

Figure 5.4: MWCNT (%5wt.): Magnetic Loss Tangent.

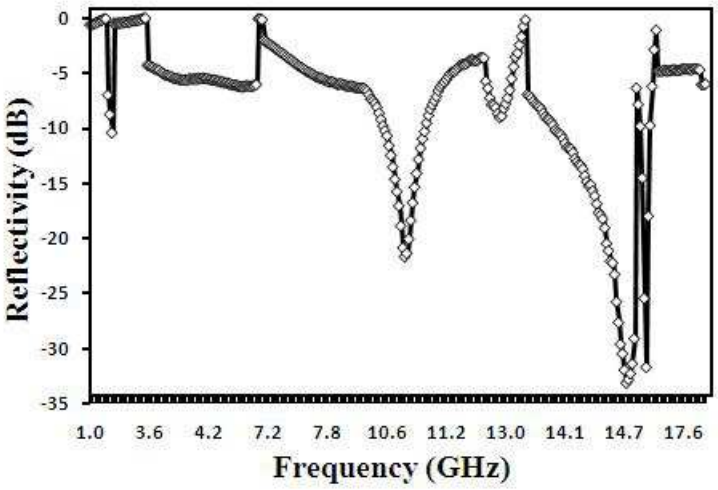

Figure 5.5: Reflectivity of a MWCNT %5wt. sample.

5.3 Fe_3O_4 (%5wt.)

The results for iron oxide are shown in Figures 5.6-5.8. Three highest peaks at 9.7GHz, 12GHz, and 13.7GHz arise primarily from the magnetic loss that can be attributed to ferrimagnetic resonance, as well as eddy current current (The skin depth for 12GHz frequency is about $3.8\mu m$. It is quite possible that since iron oxide nanoparticles were closely packed the conduction path was larger than the skin depth, so the eddy current could occur).

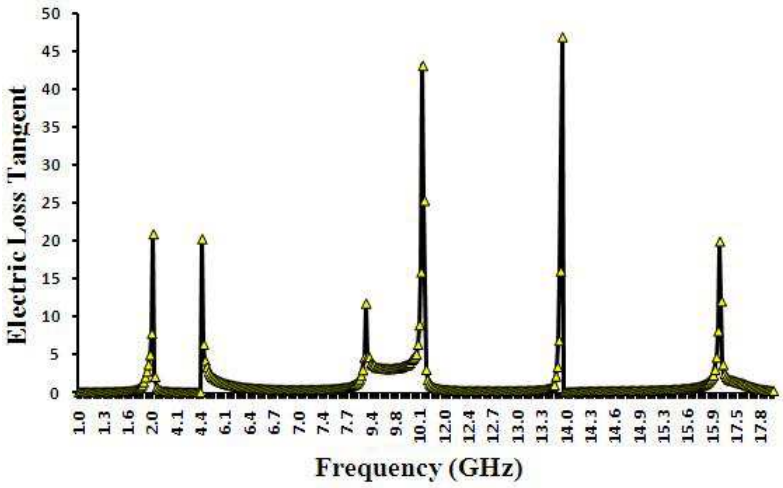

Figure 5.6: Fe_3O_4 (%5wt.): Electric Loss Tangent.

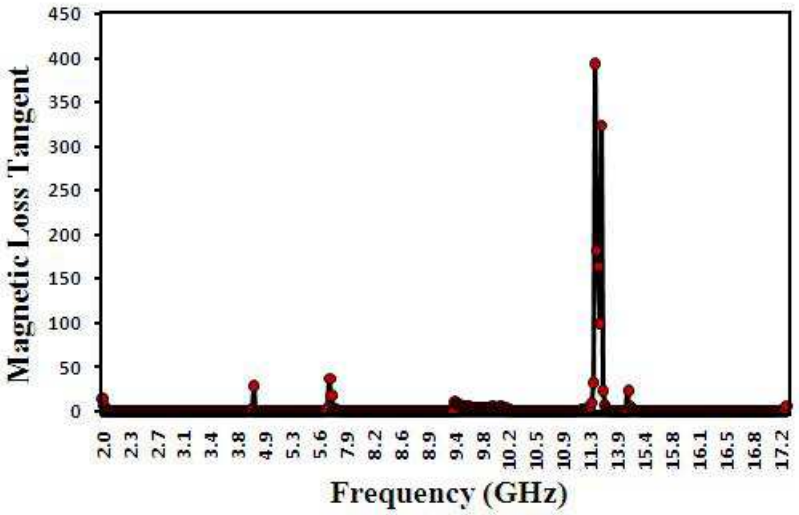

Figure 5.7: Fe_3O_4 (%5wt.): Magnetic Loss Tangent.

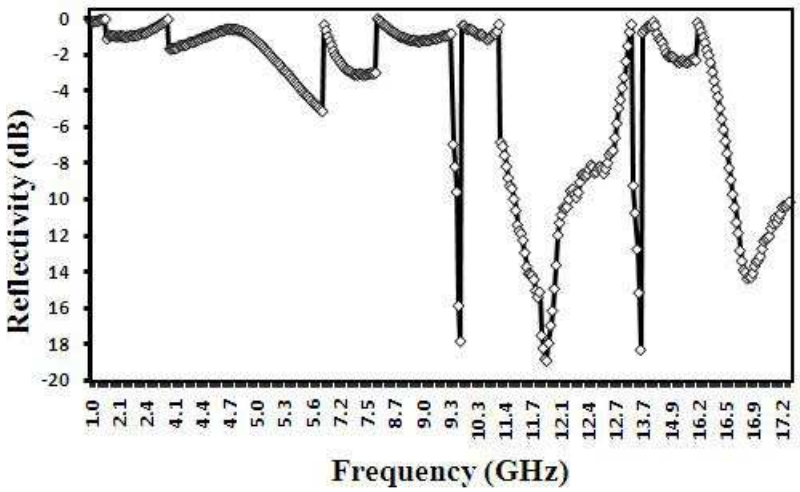

Figure 5.8: Reflectivity of a Fe_3O_4 %5wt. sample.

5.4 MWCNT (%5wt.) - Fe_3O_4 (%5wt.)

Finally, the two toroidal disks with different nanostructures were placed into the fixture. The results are shown in Figures 5.9-5.11. Here the analysis of reflectivity peaks does not yield a definite answer about the origin of the peaks. We hypothesize that the presence of several peaks below 10GHz might be due to cumulative effects of magnetic resonance losses both in iron catalyst of CNTs and Fe_3O_4 nanoparticles, while peaks at higher frequencies might be caused by the dielectric losses of MWCNTs.

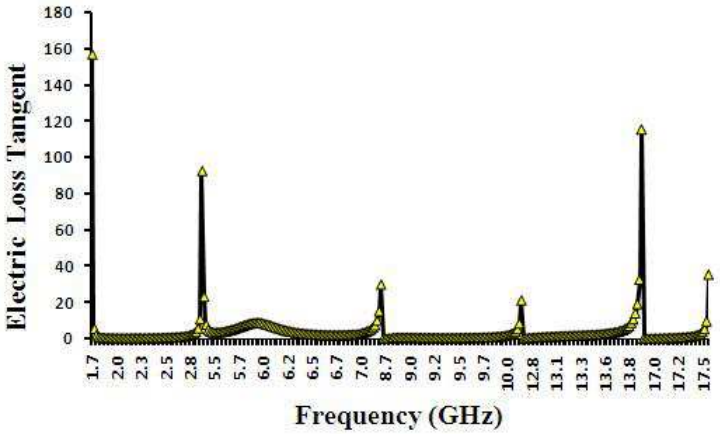

Figure 5.9: MWCNT-Fe_3O_4: Electric Loss Tangent.

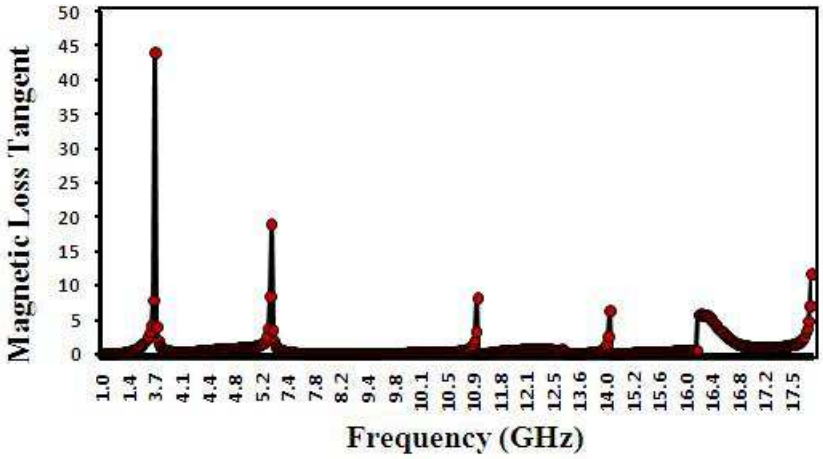

Figure 5.10: MWCNT-Fe_3O_4: Magnetic Loss Tangent.

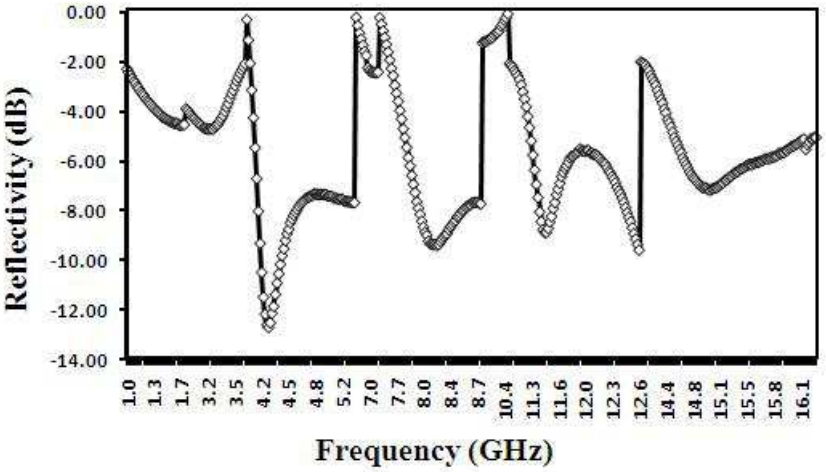

Figure 5.11: Reflectivity of a MWCNT-Fe_3O_4 sample.

6 Conclusion

In this thesis, we introduced the theory of microwave absorption for radar-absorbent materials. We showed that material's conductivity, complex permittivity, and permeability are frequency dependent parameters that govern the propagation of electromagnetic waves inside of the material. The engineering challenge is to design an absorber that provides low reflectivity (below -15dB) in a wide range of microwave frequencies and is lightweight, cheap, and easy to produce. Stacking materials with different permittivities/permeabilities on top of each other is a an effective way to build a broadband RAM. However, for classical materials the trade-off is the dramatic increase of RAM's thickness and weight. Nanomaterial due to their high aspect ratio and uniques electrical and mechanical properties could be a great alternative. We proposed a bi-layered RAM containing multi-walled carbon nanotubes and Fe_3O_4 nanoparticles. By measuring the scattering parameters of a material in a coaxial sample holder, we were able to calculate its permittivity/permeability and reflectivity based on the metal-backed absorber model[1]. Our preliminary results indicate that a sample with %5wt. MWCNTs provides a substantial absorption (-34dB) at 15GHz, and %5wt. Fe_3O_4 sample decreases reflectivity by about -18dB at 12GHz. Though the combinations of two materials did not yeild a deffiniate result, an extensive further study that involves higher concentration should provide a better understanding of the interaction of the two materials in a bi-layered configuration. Furthermore, since carbon nanotubes contained magnetic iron catalyst, there could be a potential misunderstanding of the dominant loss mechanism. Therefore, the next step could be to perform an acid treatment on carbon nanotubes to get rid off iron catalyst. Finally, varying the size of Fe_3O_4 nanoparticles during the synthesis to alter the microwave properties could be an interesting research avenue.

[1] Equations (2.29), (2.30)

Appendix A Data Formatting

```
% This function converts data from the Network Analyzer
% citi files into the text file with columns:
% Frequency | S11 Real | S11 Imaginary | S12 Real | etc..
% To make it work put the function in the current Matlab directory with the
% files to convert. Type in the Matlab command line: format_data('file
% name'); , eg. format_data('FD_NOPEN').
% Output file 'filename.txt' will be created in the same folder.
function [fData] = format_data (File)
fid = fopen(File);
tline=fgetl(fid);
% freq_zero, freq_final, freq_points should be changed according to the
% measurements settings of the network analyzer that can be found in
% the output 'citi' file (line looks like: 'SEG 1000000000 18000000000 801' )
freq_zero=1000000000;      % starting frequency
freq_final=18000000000;    % final frequency
freq_points=801;           % number of points
step=(freq_final-freq_zero)/freq_points;
fData(1,1)=freq_zero;
for i=2:freq_points
    fData(i,1)=fData(i-1,1)+step;
end;
i_par=1;
```

```
i_line=1;
while ischar(tline)
  if strcmp(tline,'BEGIN')
        for j=1:801
         a='';
         b='';
         i=1;
        tline = fgetl(fid);
        while strcmp(tline(i),',')==0
          a=strcat(a,tline(i));
          i=i+1;
        end;
        for k=i+1:length(tline)
            b=strcat(b,tline(k));
        end;
        if i_par==1
            fData(j,2)=str2double(a);
            fData(j,3)=str2double(b);

        end;
        if i_par==2
            fData(j,4)=str2double(a);
            fData(j,5)=str2double(b);
        end;
        if i_par==3
            fData(j,6)=str2double(a);
            fData(j,7)=str2double(b);
        end;
```

```
            if i_par==4
                fData(j,8)=str2double(a);
                fData(j,9)=str2double(b);
            end;
            end;
            i_par=i_par+1;
        end;
        tline = fgetl(fid);
end
fclose(fid);
save(strcat(File,'.txt'), 'fData', '-ASCII')
```

Appendix B Material Analysis

The function material_analysisV3.m creates the Graphical User Interface for the analysis of s-parameters data. A user needs to specify the text files containing s-parameters[1] for the measured material (MUT) and open measurements (OPEN), absorber thickness, De-Embedding option, and specify if the material is magnetic.

Calculate button produces four plots (permittivity, permeability, tangents loss and reflectivity VS frequency). The calculated values are also written in an Excel file, e.g for the checked De-Embedding option the output file would look like: Output-DUT FILENAME_DE-OPEN FILENAME.xlsx

The source code of the main function and the GUI screen shot are presented below.

```
function [freq,er_real,er_imag,er_abs,taner, mr_real, mr_imag,
mr_abs, tanmr,refl,cap,s11R,s11I,s21R,s21I,s12R,s12I,s22R,s22I]
=NRModel(FilePath1,FilePath2,Thickness,CheckBoxStatus1,CheckBoxStatus2)
global FILENAME1
global FILENAME2
    Data_meas=importdata(FilePath1); % import data from file
    Data_open=importdata(FilePath2);
    [m,n]=size(Data_meas);
    c = 2.99792*10^8; % speed of light
    %***** create arrays ******
    er_real =zeros(m,1);
```

[1] Use format_data.m to formate the data in columns like S11R S11I S21R S21I etc.

```
er_imag =zeros(m,1);

er_abs=zeros(m,1);

d=Thickness*10^(-3);

taner=zeros(m,1);

mr_real =zeros(m,1);

mr_imag=zeros(m,1);

mr_abs=zeros(m,1);

tanmr=zeros(m,1);

refl=zeros(m,1);

cap =zeros(m,1);

s11R=zeros(m,1);

s21R=zeros(m,1);

s12R=zeros(m,1);

s22R=zeros(m,1);

s11I=zeros(m,1);

s21I=zeros(m,1);

s12I=zeros(m,1);

s22I=zeros(m,1);

%**********************

z0=376.734;

er0=8.854*10^-12;

mr0=4*pi*10^-7;

%read frequency and s-parameters

freq=Data_meas(:,1);

s11_mag_meas=Data_meas(:,2);

s11_deg_meas=Data_meas(:,3);

s21_mag_meas=Data_meas(:,4);

s21_deg_meas=Data_meas(:,5);
```

```
s12_mag_meas=Data_meas(:,6);
s12_deg_meas=Data_meas(:,7);
s22_mag_meas=Data_meas(:,8);
s22_deg_meas=Data_meas(:,9);

% if De-Embedding is enabled than read s-parameters from file
if(CheckBoxStatus1)
s11_mag_open=Data_open(:,2);
s11_deg_open=Data_open(:,3);
s21_mag_open=Data_open(:,4);
s21_deg_open=Data_open(:,5);
s12_mag_open=Data_open(:,6);
s12_deg_open=Data_open(:,7);
s22_mag_open=Data_open(:,8);
s22_deg_open=Data_open(:,9);
end;
for k=1:m
    lamb0=c/(freq(k));
%       this is for Real/Imag s-parameter format
    s11_meas = s11_mag_meas(k)+1i*s11_deg_meas(k);
    s21_meas = s21_mag_meas(k)+1i*s21_deg_meas(k);
    s12_meas = s12_mag_meas(k)+1i*s12_deg_meas(k);
    s22_meas = s22_mag_meas(k)+1i*s22_deg_meas(k);
     % if De-Embedding is enabled than do actual De-Embedding
    if(CheckBoxStatus1)
    s11_open = s11_mag_open(k)+1i*s11_deg_open(k);
    s21_open = s21_mag_open(k)+1i*s21_deg_open(k);
    s12_open = s12_mag_open(k)+1i*s12_deg_open(k);
```

```
s22_open = s22_mag_open(k)+1i*s22_deg_open(k);
s_params_meas = [s11_meas, s12_meas; s21_meas, s22_meas];
s_params_open = [s11_open, s12_open; s21_open, s22_open];
y_params_meas = s2y(s_params_meas, 50);
y_params_open = s2y(s_params_open, 50);
y_params=y_params_meas-y_params_open;
s_params = y2s(y_params,z0);

s11=s_params(1,1);
s21=s_params(2,1);
s12=s_params(1,2);
s22=s_params(2,2);

 s11R(k)=real(s11);
 s11I(k)=imag(s11);
 s21R(k)=real(s21);
 s21I(k)=imag(s21);
 s12R(k)=real(s12);
 s12I(k)=imag(s12);
 s22R(k)=real(s22);
 s22I(k)=imag(s22);

% De-Embedding option is not enabled
else
 s11=s11_meas;
 s21=s21_meas;
 s12=s12_meas;
 s22=s22_meas;
```

```
  s11R(k)=real(s11);
  s11I(k)=imag(s11);
  s21R(k)=real(s21);
  s21I(k)=imag(s21);
  s12R(k)=real(s12);
  s12I(k)=imag(s12);
  s22R(k)=real(s22);
  s22I(k)=imag(s22);

  s_params = [s11 s12; s21 s22];
  y_params = s2y(s_params, z0);
  cap(k)=y_params(1,1)/(2*pi*freq(k));

 end;
 %Nicolson Ross Model
 V1 = s21 + s11;
 V2 = s21 - s11;
 X = (1 - V1*V2)/(V1 - V2);
if abs(X + sqrt(X^2 - 1))<=1
    G = X + sqrt(X^2 - 1);
else
    G = X - sqrt(X^2 - 1);
end;
 T=((s11+s21)-G)/(1-(s11+s21)*G);
 if(CheckBoxStatus2)
 w = 2*pi*freq(k);
 c1 = ((1 + G)/(1 - G))^2;
```

```
c2 = -(c/(w*d)*log(1/T))^2;
er = sqrt(c2/c1);
er_real(k)=real(er);
er_imag(k)=imag(er);
er_abs(k)=abs(er);
taner(k)=er_imag(k)/er_real(k);
mr = sqrt(c1*c2);
mr_real(k)=real(mr);
mr_imag(k)=imag(mr);
mr_abs(k)=abs(mr);
tanmr(k)=mr_imag(k)/mr_real(k);
else
mr=1;
mr_real(k)=real(mr);
mr_imag(k)=imag(mr);
mr_abs(k)=abs(mr);
tanmr(k)=mr_imag(k)/mr_real(k);
er=((1 - G)^2/(1 + G)^2);
er_real(k)=real(er);
er_imag(k)=imag(er);
er_abs(k)=abs(er);
taner(k)=er_imag(k)/er_real(k);
end;
r = sqrt(mr/er)*tanh( 1i*(2*pi/c)*freq(k)*d*sqrt(mr*er) );
refl (k) = 20*log10(abs( (r-1)/(r+1) ));

% Create xlsx file and write data
if(CheckBoxStatus1)    % if De-Embedding is enabled that include the OPEN file
```

```
OutFile=strcat('Output-',FILENAME1,'_DE-',FILENAME2,'.xlsx');


else                    % De-Embedding option is not enabled
OutFile=strcat('Output-',FILENAME1,'.xlsx');
end
Header={'Freq.␣(Hz)', 'e␣Real','e␣Imaginary','Abs(e)','Loss␣Tan␣e','u␣Real',
'u␣Imaginary','Abs(u)','Loss␣Tan␣u','Reflectivity','Capacitance','s11R','s11I',
's21R','s21I','s12R','s12I','s22R','s22I'};
xlswrite(OutFile,Header,'A1:S1');
xlswrite(OutFile,freq,strcat('A2:A',num2str(m+1)));
xlswrite(OutFile,er_real,strcat('B2:B',num2str(m+1)));
xlswrite(OutFile,er_imag,strcat('C2:C',num2str(m+1)));
xlswrite(OutFile,er_abs,strcat('D2:D',num2str(m+1)));
xlswrite(OutFile,taner,strcat('E2:E',num2str(m+1)));
xlswrite(OutFile,mr_real,strcat('F2:F',num2str(m+1)));
xlswrite(OutFile,mr_imag,strcat('G2:G',num2str(m+1)));
xlswrite(OutFile,mr_abs,strcat('H2:H',num2str(m+1)));
xlswrite(OutFile,tanmr,strcat('I2:I',num2str(m+1)));
xlswrite(OutFile,refl,strcat('J2:J',num2str(m+1)));
xlswrite(OutFile,cap,strcat('K2:K',num2str(m+1)));
xlswrite(OutFile,s11R,strcat('L2:L',num2str(m+1)));
xlswrite(OutFile,s11I,strcat('M2:M',num2str(m+1)));
xlswrite(OutFile,s21R,strcat('N2:N',num2str(m+1)));
xlswrite(OutFile,s21I,strcat('O2:O',num2str(m+1)));
xlswrite(OutFile,s12R,strcat('P2:P',num2str(m+1)));
xlswrite(OutFile,s12I,strcat('Q2:Q',num2str(m+1)));
xlswrite(OutFile,s22R,strcat('R2:R',num2str(m+1)));
xlswrite(OutFile,s22I,strcat('S2:S',num2str(m+1)));
```

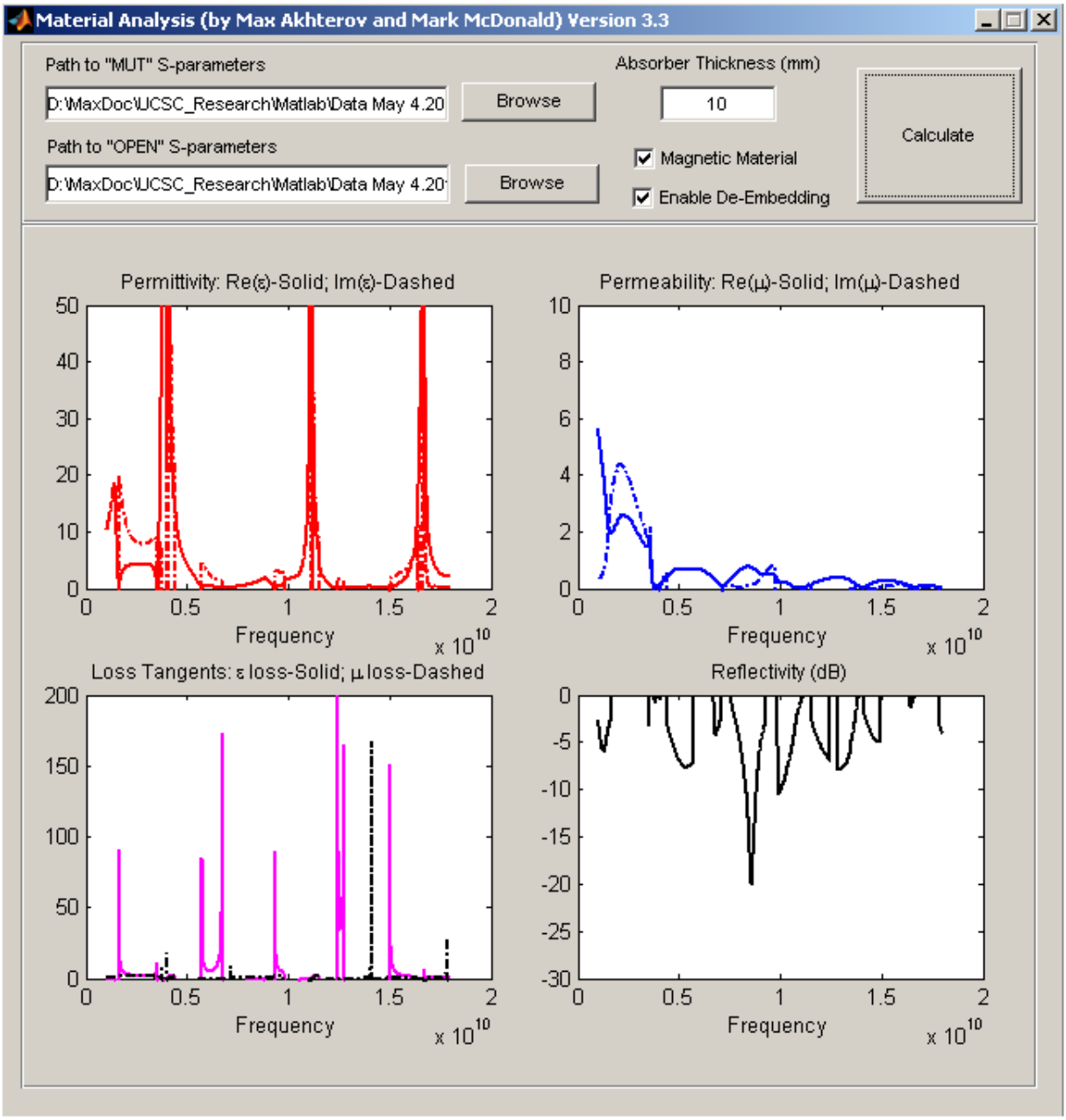

Figure B.1: Material Analysis GUI.

Bibliography

[1] E.F. Knott, J.F. Shaeffer, M.T. Tuley, *Radar Cross Section*, 2nd ed. (Artech House, Boston, 1993).

[2] S.J. Orfanidis,*Electromagnetic Waves and Antennas*, (Rutgers University, 1999).

[3] D. Griffiths,*Introduction to electrodynamics*, 3rd ed. (Prentice-Hall of India, New Delhi, 2008).

[4] R. Diaz,http://www.microwaves101.com/encyclopedia/absorbingradar3.cfm.

[5] M. Hill, *The Microwave Palaeointensity Technique and its Application to Lava*, PhD. Thesis, (University of Liverpool, 2000).

[6] A.J. Moulson and J. M. Herbert,*Electroceramics: Materials, Properties, Applications*, 2nd ed. (Wiley, West Sussex, 2003).

[7] Application Note 1217-1, *Basics of Measuring the Dielectric Properties of Materials*, Agilent Technologies, Inc., 2006.

[8] C. Kittel,*Physical Review*, **73**, 2 (1948).

[9] J.L. Snoek,*Physica (Amsterdam)*, **14**, 207 (1948).

[10] L. Landau and E.Lifshitz, *Phys. Z. Soviet Union*, **8**, 153 (1935).

[11] J. Cao, *et. al.*, *J. Phys. Chem. B*, **113**, 4642 (2009).

[12] S. Iijima,*Nature*, **354**, 56 (1991).

[13] H. Baughman, *Science*,**297**, 787 (2002).

[14] S. Lee, *et. al.*, *Composite Structures*, **76**, 397 (2006).

[15] R. Che, *et. al.*,*Adv. Mater.*, **16**, 5 (2004).

[16] D. Zhao,*et. al.*,*Materials Science and Engineering B*, **150**, 105 (2008).

[17] A. Jozefczak, *J. Magn. Magn. Mater.*, **293**, 240 (2005).

[18] Y. Zhang, *J. Colloid Interface Sci.*, **283**, 352 (2005).

[19] H. Iida,*et. al.*, *Journal of Colloid and Interface Science*, **314**, 274 (2007).

[20] H. Zheng,*et. al.*,*Hyperfine Interact*, **189**, 131 (2009).

[21] X.F. Zhang,*et. al.*,*Appl. Phys. Lett.*, **89**, 053115 (2006).

[22] M. Hergert,*et. al.*,http://mars.mines.edu/diaperm/system.htm.

[23] P-N Designs, Inc., http://www.microwaves101.com/encyclopedia/sparameters.cfm.

[24] A. M. Nicolson and G. F. Ross,*IEEE Trans. on Instrum. Meas.*, **IM-19**, 4 (1970).

[25] W.B. Weir, *Proc. IEEE*, **62**, 33 (1974)